

Early Dust Formation and a Massive Progenitor for SN 2011ja?

J.E. Andrews^{1*}, Kelsie M. Krafton², Geoffrey C. Clayton², E. Montiel², R. Wesson³,
Ben E.K. Sugerman⁴, M.J. Barlow⁵, M. Matsuura⁶, & H. Drass⁷

¹*Steward Observatory, University of Arizona, 933 North Cherry Avenue, Tucson, AZ 85721, USA*

²*Department of Physics and Astronomy, Louisiana State University, 202 Nicholson Hall, Baton Rouge, LA 70803, USA*

³*European Southern Observatory, Alonso de Cordova 3107,19001 Casilla, Santiago, Chile*

⁴*Department of Physics and Astronomy, Goucher College, 1021 Dulaney Valley Rd., Baltimore, MD 21204*

⁵*Department of Physics and Astronomy, University College London, Gower Street, London WC1E 6BT*

⁶*School of Physics and Astronomy, Cardiff University, Cardiff CF24 3AA, UK*

⁷*Astronomisches Institut, Ruhr-Universität Bochum, Universitätsstraße 150, 44780 Bochum, Germany*

Accepted 0000, Received 0000, in original form 0000

ABSTRACT

SN 2011ja was a bright ($I = -18.3$) Type II supernova occurring in the nearby edge on spiral galaxy NGC 4945. Flat-topped and multi-peaked $H\alpha$ and $H\beta$ spectral emission lines appear between 64 - 84 days post-explosion, indicating interaction with a disc-like circumstellar medium inclined 30-45 degrees from edge-on. After day 84 an increase in the H- and K-band flux along with heavy attenuation of the red wing of the emission lines are strong indications of early dust formation, likely located in the cool dense shell created between the forward shock of the SN ejecta and the reverse shock created as the ejecta plows into the existing CSM. Radiative transfer modeling reveals both $\approx 1.5 \times 10^{-4} M_{\odot}$ of pre-existing dust located $\sim 10^{16.7}$ cm away and $\approx 5 \times 10^{-5} M_{\odot}$ of newly formed dust. Spectral observations after 1.5 years reveal the possibility that the fading SN is located within a young (3-6 Myr) massive stellar cluster, which when combined with tentative ^{56}Ni mass estimates of $0.2 M_{\odot}$ may indicate a massive ($\geq 25 M_{\odot}$) progenitor for SN 2011ja.

Key words: circumstellar matter — stars: winds, outflows — supernovae: general — supernovae: individual (SN 2011ja)

1 INTRODUCTION

Type IIP, the most common type of core collapse supernovae (CC-SNe), have broad ($\sim 10^4$ km s⁻¹) hydrogen emission lines along with a near constant “plateau” of optical luminosity throughout the first ~ 100 days. The widely accepted progenitors of Type IIP SNe, red supergiants (RSGs), have masses ranging between ~ 9 - $25 M_{\odot}$ and mass loss rates of $\sim 10^{-6}$ to $10^{-4} M_{\odot} \text{ yr}^{-1}$ (Chevalier et al. 2006; Maun & Josselin 2011). Type IIn SNe also show broad hydrogen emission, but, in addition, they show narrow (~ 100 km s⁻¹) hydrogen emission due to ionization of the surrounding, dense pre-existing circumstellar material (CSM). These SNe likely have more massive progenitors such as Luminous Blue Variables (LBV), or Wolf-Rayet (WR) stars that can have mass loss rates which are orders of magnitude larger, 10^{-5} to $10^{-2} M_{\odot} \text{ yr}^{-1}$ (Kiewe et al. 2012; Smith et al. 2011, 2014). Whether Type IIP or Type IIn, these massive star progenitors can undergo periods of dramatic mass loss prior to explosion which has a direct impact on the SN evolution. Over the past decade we have seen numerous observational signatures of the SN ejecta interacting with previously shed lay-

ers, anywhere from hours to years after explosion (Leonard et al. 2000; Andrews et al. 2010; Fransson et al. 2014; Smith et al. 2015; Maeda et al. 2015, for example). By observing the SN-CSM interaction we can get a better understanding of pre-supernova mass loss, pathways of dust production, and the link between progenitor and SN type.

Due to their short lifetimes and ability to return material back to the ISM quickly, CCSNe are the likely culprits for the dust production in dusty high-z galaxies (Gall et al. 2011; Dwek et al. 2014). This is a double-edged sword, as they are also efficient destroyers of dust, at least in present day galaxies (Temim et al. 2015). Although Slavin et al. (2015) propose effective SN dust destruction, but only within a subset of the appropriate assumed parameters. Many recent studies of nearby CCSNe have searched for signatures of dust formation and estimated the dust masses. The results of these studies indicate small amounts of newly-formed dust, 10^{-2} - $10^{-4} M_{\odot}$ (Elmhamdi et al. 2003; Sugerman et al. 2006; Meikle et al. 2007; Kotak et al. 2009; Andrews et al. 2010, for example), much less than the 0.1 - $1 M_{\odot}$ needed to account for the excess of dust seen in the early Universe. Within the past few years, far-IR studies have revealed a few sources which may hold promise to unlocking the dust mystery. Herschel observations of

* Email: jandrews@as.arizona.edu

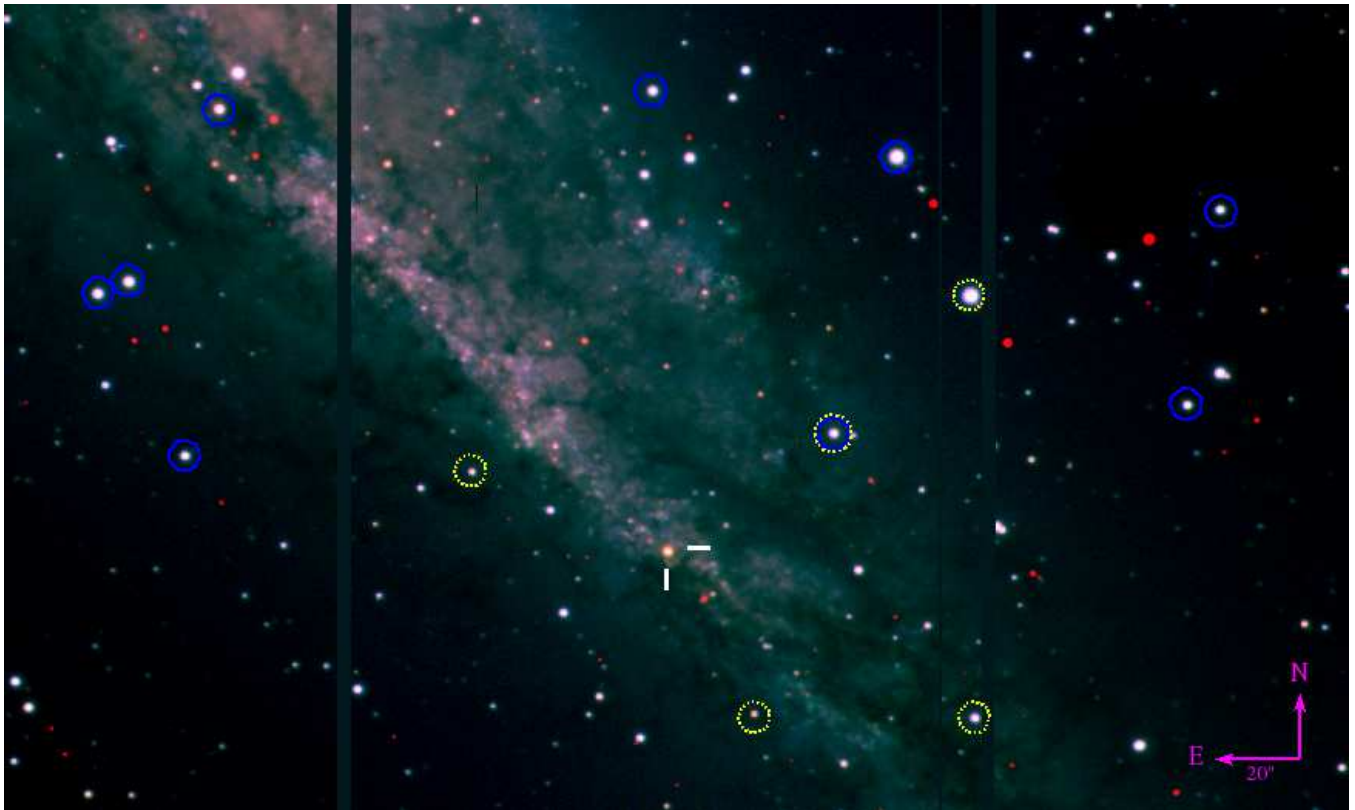


Figure 1. Color composite Gemini/GMOS image of SN 2011ja (indicated in white). Optical standards (Table 3) are indicated by blue solid circles, NIR standards (Table 4) by dashed yellow circles.

three nearby young supernova remnants indicate the presence of $0.1 M_{\odot}$ of cool dust in Cas A (Barlow et al. 2010), $0.4 - 0.7 M_{\odot}$ of cool dust in the ejecta of SN 1987A (Matsuura et al. 2011, 2015) and $0.18-0.27 M_{\odot}$ of cool dust in the Crab Nebula (Gomez et al. 2012; Owen & Barlow 2015). Recent SOFIA observations of a supernova remnant at the center of the Milky Way revealed $0.02 M_{\odot}$ of warm (100 K) dust, which also has seemed to have survived the passing of the reverse shock (Lau et al. 2015). This strongly suggests that almost all of the dust in SNe is formed after > 1000 days (Wesson et al. 2015; Bevan & Barlow 2015). While reservoirs of cold dust may help solve this problem, there is a growing body of evidence that grain growth may be occurring in the ISM enriched by these early SNe and could be the main site for dust production at high- z (Michałowski 2015). However, a plausible mechanism for growing refractory grains in the ISM has yet to be identified.

Observational signatures of dust formation in CCSNe manifest themselves in several different forms. The optical luminosity will decrease while almost simultaneously the NIR will increase as the dust grains absorb the shorter wavelength light and re-emit it in the IR. The grain formation will also alter the optical spectra, creating asymmetric and blue-shifted lines as the dust grains attenuate the red, receding side of the ejecta preferentially. This observational evidence of dust formation has now been seen in numerous SNe, including the nearby and well-studied SN 1987A (Lucy et al. 1989; Wooden et al. 1993), SN 2003gd (Sugerman et al. 2006; Meikle et al. 2007), SN 2004et (Sahu et al. 2006; Kotak et al. 2009) and many others. While it was initially believed that the dust grains could only condense 300-600 days after explosion, when the ejecta had expanded and cooled, there have been more and more confirmed cases of dust forming much ear-

lier, within ~ 100 days of explosion. This can occur due to shock interaction with nearby CSM creating an area between the forward and reverse shocks with temperatures and densities appropriate for grain growth, this area is known as the cool dense shell (CDS). For example SN 1998S showed dust formation signatures between days 140 - 268 (Leonard et al. 2000), and SN 2005ip appears to have formed dust both in the CDS between day 75-150 and then again in the ejecta after day 750 (Smith et al. 2009; Fox et al. 2009). The bright IIn SN 2010jl shows continuous dust formation between 40 and 240 days (Gall et al. 2014). Although not classified as Type IIn, the Type Ib/c SN 2006jc also formed dust via CSM interaction between 50 - 75 days post-explosion (Mattila et al. 2008; Smith et al. 2008) and the Type IIP SN 2007od formed dust sometime between day 120 - 230 through the same mechanism (Andrews et al. 2010). As we will present below, with more and more long-term monitoring of CCSNe, there seems to be evidence of non-Type-IIn SNe exhibiting signs of CSM interaction, even months after explosion. This not only allows a separate channel for dust formation in CC-SNe, but can also reveal important properties of SN evolution.

SN 2011ja was discovered in NGC 4945, an edge-on spiral (Figure 1) located at a distance of 3.36 ± 0.09 Mpc (Mouhcine et al. 2005). NGC 4945 is one of the closest Milky Way analogs with a near solar metallicity, particularly at increasing distances from the galactic center where the supernova is located (Stanghellini et al. 2015). This is of importance, particularly in dust formation, as higher metallicity galaxies tend to be able to produce higher dust masses (Draine et al. 2007; Galametz et al. 2011). On 2011 December 19, optical spectra obtained of the object indicated that it was a Type II supernova which most closely matched SN 2004et about a week after maximum (Monard et al. 2011), al-

though maximum optical light of SN 2011ja does not appear to have been achieved until \sim 2012 January 14 (Figure 2). Radio observations presented in Chakraborti et al. (2013), further suggest an explosion date of 2011 December 12 (JD 2455907). Therefore, throughout this paper we choose 2011 December 12 as day 0 for SN 2011ja, and day 34 as the date of maximum light. In Section 2, we discuss the data reductions and present a comprehensive analysis of these data in Section 3. Section 4 contains a discussion of the implications of the data, and Section 5 includes analysis in regards to dust formation, CSM location, and progenitor characteristics. Finally, in Section 6 we briefly summarize the significant results of the paper.

2 OBSERVATIONS AND DATA REDUCTION

Optical imaging and spectra were obtained with GMOS/Gemini South (GS-2012A-Q-79, GS-2013-Q-93, PI Andrews). A Color composite Gemini/GMOS image of SN 2011ja is shown in Figure 1, and a summary of observations and resultant photometry in Table 1. The $g'r'i'$ images were reduced and stacked using the IRAF¹ *gemini* package. The instrumental $g'r'i'$ magnitudes were transformed to standard Johnson-Cousins VRI using tertiary standards created from stars in the field (Figure 1 and Table 2) and transformations presented in Welch et al. (2007). Uncertainties were calculated by adding in quadrature the transformation uncertainty quoted in Welch et al. (2007), photon statistics, and the zero point deviation of the standard stars for each epoch. Figures 2 and 3 show the resultant light curves.

For each GMOS/Gemini South epoch, three spectra of 900s were obtained in semester 2012A and six spectra of 900s were obtained in semester 2013A. The spectra were obtained in longslit mode using grating B600 and a slit width of $0''.75$. With a resolving power $R = 1688$, this corresponds to a velocity resolution of $\sim 180 \text{ km s}^{-1}$. Central wavelengths of 5950, 5970, and 5990 Å were chosen to prevent important spectral features from falling on chip gaps. A 2×2 binning in the low gain setting was used. Spectra were reduced using the IRAF *gemini* package. The sky subtraction regions were determined by visual inspection to prevent contamination from material not associated with the SN, and the spectra were extracted using 15 rows centered on the SN. The spectra from each individual night were averaged and have been corrected for the radial velocity of NGC 4945 (460 km s^{-1}) obtained from narrow line emission (Monard et al. 2011). Spectrophotometric standards were not taken as part of our Gemini program but are taken at least once per semester. For each of our observations we have flux calibrated our spectra using the spectrophotometric standard that is closest in date to the observation. The final spectra are presented in Figures 4 and 5.

Seven epochs of JHK_s imaging, spanning 8 to 272 days post-explosion, were obtained from NTT/SOFI data made available on the ESO archive (184.D-1140(N), PI Benetti). A summary of the epochs and resultant photometry is presented in Table 3 and shown in Figure 2. Observations were taken with a pixel scale of $0.288''/\text{pixel}$ in a four-point dither pattern for background subtraction. Images were corrected for crosstalk and background contamination using IRAF scripts provided on the SOFI website then re-

Table 1. Gemini/GMOS Photometry of SN 2011ja

| Day | JD | V | R | I |
|-----|---------|------------------|------------------|------------------|
| 84 | 2455991 | 17.20 ± 0.08 | 14.87 ± 0.06 | 13.76 ± 0.06 |
| 112 | 2456019 | 18.00 ± 0.10 | 15.71 ± 0.06 | 14.62 ± 0.06 |
| 159 | 2456066 | 18.37 ± 0.05 | 16.10 ± 0.05 | 15.03 ± 0.04 |
| 450 | 2456357 | 19.88 ± 0.10 | 18.42 ± 0.11 | 17.64 ± 0.10 |
| 508 | 2456415 | 19.95 ± 0.10 | 18.76 ± 0.12 | 17.88 ± 0.10 |
| 807 | 2456714 | 19.74 ± 0.11 | 18.61 ± 0.11 | 18.05 ± 0.08 |

Table 2. Tertiary VRI Standards for NGC 4945

| Star | α (J2000) $196^h +$ | δ (J2000) $-49^\circ +$ | V | R | I |
|------|-------------------------------|-----------------------------------|-------|-------|-------|
| A | .341633 | .495212 | 16.30 | 15.42 | 14.98 |
| B | .350917 | .506569 | 15.39 | 14.90 | 14.73 |
| C | .353678 | .507214 | 15.70 | 14.43 | 14.93 |
| D | .345111 | .517944 | 16.31 | 16.26 | 15.67 |
| E | .240586 | .501742 | 16.44 | 15.82 | 15.57 |
| F | .243756 | .514639 | 16.60 | 16.11 | 15.56 |
| G | .297883 | .493965 | 15.85 | 14.56 | 15.12 |
| H | .279450 | .516431 | 16.28 | 14.88 | 15.45 |
| I | .297790 | .494104 | 16.77 | 15.81 | 16.02 |

Photometry is from NOMAD and DENIS catalogs.

duced, aligned, and stacked using standard IRAF techniques. Differential aperture photometry was performed using the 2MASS standards listed in Table 4. On 2011 December 17 (Day 15) and 2012 April 30 (Day 113) we also obtained JHK_s imaging from the 0.8m Infrared Imaging System (IRIS) telescope at Cerro Armazones Observatory, Chile (operated by the Astronomical Institute of the Ruhr-Universität Bochum and the Universidad Católica del Norte.) Aperture photometry was also performed using the standards presented in Table 4. Additional low resolution optical spectra for days 64 and 237, observed with NTT/EFOSC, were also obtained from the ESO archive (184.D-1151(Z), PI Benetti). Observations were taken using a slit width of $1''.0$ and grism 13, which has a resolution of $\sim 2.8 \text{ \AA}/\text{pixel}$. Standard IRAF reduction procedures were applied, and background subtraction was done using the same area as for the GMOS spectra. Flux calibration was achieved using spectrophotometric standards taken on the night of observation.

Spitzer IRAC (3.6 and $4.5 \mu\text{m}$) images were obtained at four epochs from day 105-857. The images were mosaicked and resampled using standard MOPEX procedures to improve photometric quality. A summary of the observations and fluxes are shown in Table 3. PSF photometry was performed using the Point Response Functions (PRF) developed for IRAC. Additional mid-IR observations at 18.72 and $10.77 \mu\text{m}$ were obtained with VLT/VISIR (288.D-5031(A), PI Wesson) on 2012 February 26 (day 76) and March 14 (day 93), respectively. For the B10.7 filter a total 3600s was taken on target as was 7200s for the Q2 filter. Both observations resulted in a non-detection, so only upper limits can be inferred. These are 2 mJy for $10.7 \mu\text{m}$ and 10 mJy for $18.72 \mu\text{m}$.

¹ IRAF is distributed by the National Optical Astronomical Observatory, which is operated by the Association of Universities for Research in Astronomy, Inc., under cooperative agreement with the National Science Foundation.

Table 3. Near- and Mid- IR Photometry of SN 2011ja

| Day | JD | J | H | K | 3.6 μm (mJy) | 4.5 μm (mJy) |
|-----|---------|------------------|------------------|------------------|-------------------------|-------------------------|
| 8 | 2455915 | 11.46 \pm 0.05 | 11.85 \pm 0.03 | 10.76 \pm 0.06 | | |
| 15 | 2455922 | 11.12 \pm 0.04 | 10.93 \pm 0.04 | 10.32 \pm 0.04 | | |
| 40 | 2455947 | 10.78 \pm 0.03 | 10.29 \pm 0.03 | 9.92 \pm 0.06 | | |
| 65 | 2455972 | 11.15 \pm 0.03 | 10.63 \pm 0.02 | 10.20 \pm 0.07 | | |
| 93 | 2456000 | 12.59 \pm 0.03 | 12.02 \pm 0.04 | 11.60 \pm 0.06 | | |
| 105 | 2456012 | - | - | - | 12.54 \pm 0.29 | 14.35 \pm 0.24 |
| 113 | 2456020 | 12.85 \pm 0.10 | 12.22 \pm 0.10 | 11.60 \pm 0.15 | | |
| 121 | 2456028 | 13.12 \pm 0.02 | 12.45 \pm 0.04 | 11.87 \pm 0.06 | | |
| 243 | 2456150 | 14.11 \pm 0.11 | 12.65 \pm 0.07 | 11.49 \pm 0.07 | | |
| 272 | 2456179 | 14.39 \pm 0.04 | 12.91 \pm 0.02 | 11.63 \pm 0.04 | | |
| 486 | 2456393 | - | - | - | 13.48 \pm 0.29 | 15.32 \pm 0.24 |
| 637 | 2456544 | - | - | - | 10.16 \pm 0.26 | 11.63 \pm 0.22 |
| 857 | 2456764 | - | - | - | 7.79 \pm 0.20 | 8.17 \pm 0.17 |

Table 4. Tertiary 2MASS Standards for NGC 4945

| Star | α (J2000) 196 ^h + | δ (J2000) -49 ^o + | J | H | K |
|------|--|--|-------|-------|-------|
| 1 | .265558 | .507378 | 12.68 | 12.44 | 12.38 |
| 2 | .279346 | .516434 | 14.77 | 14.35 | 14.27 |
| 3 | .264956 | .535126 | 15.08 | 14.64 | 14.55 |
| 4 | .316055 | .519047 | 15.79 | 15.01 | 14.87 |
| 5 | .287417 | .534851 | 15.50 | 14.90 | 14.84 |

3 ANALYSIS

3.1 Internal Extinction

The initial discovery spectrum, shown in Figure 4, suggested a large amount of extinction toward SN 2011ja (Monard et al. 2011). The Milky Way foreground is only $A_V=0.48$ mag (Schlafly & Finkbeiner 2011) so much of the extinction is internal to NGC 4945, which is not unexpected as extinction estimates along its galactic plane are $A_V > 11-13$ (Marconi et al. 2000). In order to determine an accurate extinction value for SN 2011ja, we have employed a variety of tests. Because of the low recession velocity of the galaxy (450 km s^{-1}) the use of Na ID doublet was insufficient for this galaxy due to the blending of internal and external Na absorption lines. This is not necessarily a hindrance, as it is still under debate whether this method is acceptable for SNe (Poznanski et al. 2011, 2012), especially in the presence of circumstellar material. Therefore, we compared our unreddened, early-time spectra with optical spectra of SN 2004et, a prototypical Type IIP, from similar epochs and applied extinction corrections until the spectra were coincident. SN 2004et has an $E(B-V) = 0.43$ (Sahu et al. 2006), and comparisons on both day 7 and day 84 yield a total $E(B-V)=1.8$ in SN 2011ja, using the reddening law of CCM (Cardelli et al. 1989). Throughout this paper we use a value of total reddening, foreground to SN2011ja, to be $E(B-V) = 1.8$.

As a second method and sanity check, we measured the relative line strengths of the $H\alpha$ and $H\beta$ nebular emission, assuming both Case A and Case B recombination in the HII region surrounding the SN, as these are the two extremes of hydrogen recombination, and the area surrounding SN 2011ja must lie somewhere in between. In the absence of reddening we would expect a ratio of 2.85 for Case B and 1.91 for Case A, but we find a ratio closer to 17.25 suggesting $1.64 < E(B-V) < 2.01$ (Seaton 1979). This is in

reasonable agreement with comparison to the SN 2004et spectra. When we measure this ratio on day 159, $E(B-V)$ has increased to 2.10, indicating an additional increase in A_V of 0.55 mag between these two dates, assuming $R_V = 3.1$. As we will discuss below, this is likely due to early-dust formation.

3.2 Optical Lightcurve Evolution

Figure 2 shows the VRI evolution of SN 2011ja between days 28 - 1138. The I-band AAVSO observations up to day 77 indicate that the SN may have been increasing in luminosity since discovery and reached a maximum brightness on 2012 January 14, day 34. Shown in detail in Figure 3, the plateau phase only lasted for ~ 35 days, with a decline rate of $0.01 \text{ mag day}^{-1}$. The drop into the radioactive decay portion of the light curve that begins on day ~ 70 , lasted only 15 days with a ΔI of 1 magnitude, which was similar for the other optical bands. It is possible that the transitional phase lasted until day 112, and if this is the case, the SN faded by 1.8 mags in 42 days (a rate of $0.04 \text{ mag day}^{-1}$). We have reason to believe, as explained below, that the start of the radioactive decay phase was in fact around the time of our first GMOS observation of SN 2011ja on day 84.

Comparison with the lightcurves of other Type II SNe shown in Figure 3, particularly after day 50, shows that SN 2011ja may lie somewhere between a Type IIP and a Type IIL classification-wise. The blurring between “plateau” and “linear” designations of Type II SNe is becoming more common as the sample of well studied objects increases, with a survey of hydrogen rich SNe presented by Anderson et al. (2015) concluding that there are not two distinct classes, but rather a continuum based most strongly on the envelope mass at explosion. This is somewhat at odds with Arcavi et al. (2012) who make a contrary claim that there are distinct groups based on progenitor types. The short plateau duration, the absolute magnitude at maximum ($I = -18.3$), and the steep drop into the radioactive decay phase all point to a CCSN with a smaller hydrogen envelope, which we will discuss in more detail below.

Assuming the radioactive decay phase started on day 84, the V-band magnitudes should then be 17.47 on day 112 and 17.92 on day 159 if the only energy source is the decay of ^{56}Co (dashed line in Figure 2). This is roughly 0.5 magnitudes brighter than the observed magnitude, requiring an increase in optical depth (τ) of 0.5 between day 84 and 112 to account for the magnitude deficit. Modeling of the optical and IR photometry lend credence to this hypothesis, and as we will show in Section 4, radiative transfer modeling

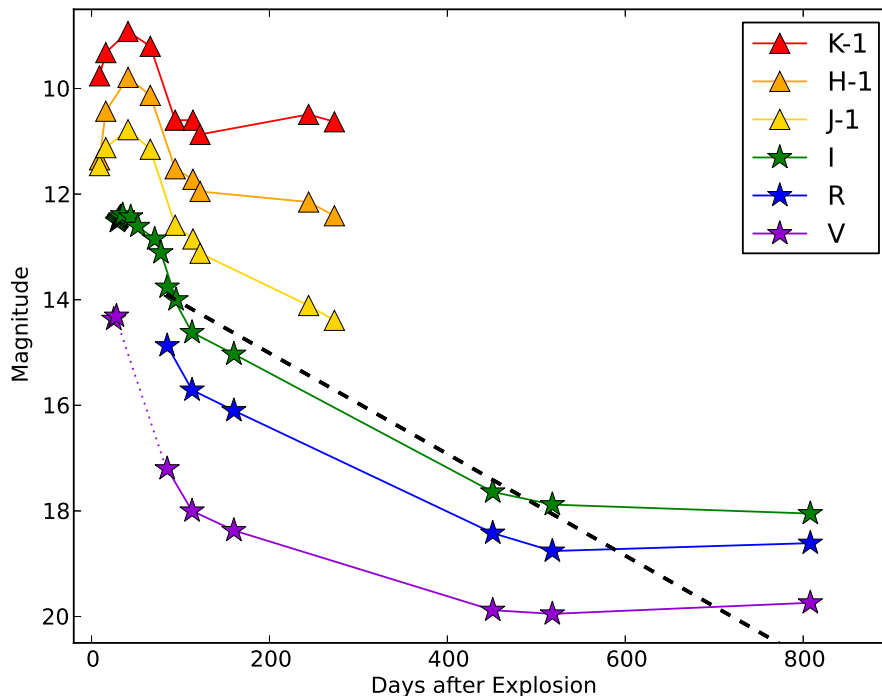


Figure 2. Optical and IR light curves of SN 2011ja from values listed in Tables 1 and 3. The NIR curves have been shifted up one magnitude for clarity. V and I photometry prior to day 84 has been obtained from AAVSO. The dashed line follows the decay of ^{56}Co .

shows that there is a substantial increase in τ_V between day 105 and day 486. By itself this does not necessarily confirm an increase of extinction prior to day 159, but in tandem with the optical spectroscopy presented in the next section, we have sufficient reason to believe new dust was being formed within 100 days of explosion in SN 2011ja.

Alternatively if the radioactive decay phase is assumed to begin on day 112, the SN does not suffer from any increased extinction and behaves as expected until ~ 400 days, when the luminosity levels out through our last observation on day 857. This late-time plateau can be caused by various physical mechanisms, notably a scattered-light echo, shock-interaction, or ambient light from the parent stellar cluster. These scenarios are discussed in detail in Section 5.2.

3.3 Spectra

Early-time spectra of SN 2011ja show a prototypical Type II supernova (Figure 4, Day 7), with blue-shifted $\text{H}\alpha$ and $\text{H}\beta$ emission lines, peaking at -3500 km s^{-1} and -3000 km s^{-1} , respectively, and very little else. While most other SNe show a very blue continuum at these early times, the high reddening towards SN 2011ja represses this feature. This is further exemplified by a strong Na I D absorption feature present around 5900\AA . A high-velocity feature (HV) may also be present in the Day 7 spectrum at $\sim 13,700 \text{ km s}^{-1}$, likely due to flash-heated unshocked pre-explosion mass loss from the progenitor star (Chugai et al. 2007).

Our first GMOS spectra of SN 2011ja was obtained on day 84, when the multi-component hydrogen lines that seem to appear in the day 64 spectra are now prevalent (Figure 5). Blue-shifted

and red-shifted peaks are seen in $\text{H}\alpha$ at -1400 km s^{-1} , and 2900 km s^{-1} , in addition to the narrow nebular line at 0 km s^{-1} . There is also a possible tertiary peak on the red side at 1700 km s^{-1} . The $\text{H}\beta$ emission shows peaks at -2100 km s^{-1} and 3100 km s^{-1} , but not the existence of a second red-shifted component. We cannot ascertain if a double-peaked structure exists in the He I $\lambda 5876$ line due to the blending with the Na I D doublets from local and host galaxy extinction. Multi-peaked asymmetric hydrogen lines have been seen in other SNe, such as SN 1993J (Matheson et al. 2000), SN 1998S (Leonard et al. 2000), SN 2004dj (Chugai et al. 2007), SN 2007od (Andrews et al. 2010), SN 2009ip (Mauerhan et al. 2014), and PTF11iqb (Smith et al. 2015), and are mostly attributed to a toroidal or disc geometry of surrounding CSM material. Comparison with models presented in Fransson et al. (2005) indicate that the CSM around SN 2011ja may be represented by a torus inclined between 30-60 degrees with an angular thickness between 30 and 50 degrees.

Other broad nebular lines such as Ba II $\lambda 6142$, [Sc II] $\lambda 5527$, $\lambda 5658$, and $\lambda 6246$, and [O I] $\lambda \lambda 6300, 6363$ are dominant in the nebular spectra. Fe II $\lambda \lambda 4924, 5169$ may also be present and somewhat blended with $\text{H}\beta$ and other Sc lines. An intermediate-width component of [O III] $\lambda 5007 \text{ \AA}$ seems to appear at this time as well, and persists until our last spectra on day 807. Alternatively, this could be a -735 km s^{-1} blue-shifted peak of Fe $\lambda 5018 \text{ \AA}$. If this is the case, then the red emission peak of $\text{H}\beta$ is likely blended with a similarly blue-shifted component of Fe $\lambda 4924 \text{ \AA}$. The only other published example of broad [O III] emission is in the well-studied Type II_n 1995N (Fransson et al. 2002). In that object, lines of a similar width (1500 km s^{-1}) were seen, the only difference being in SN 1995N they showed a much more boxy profile, similar to

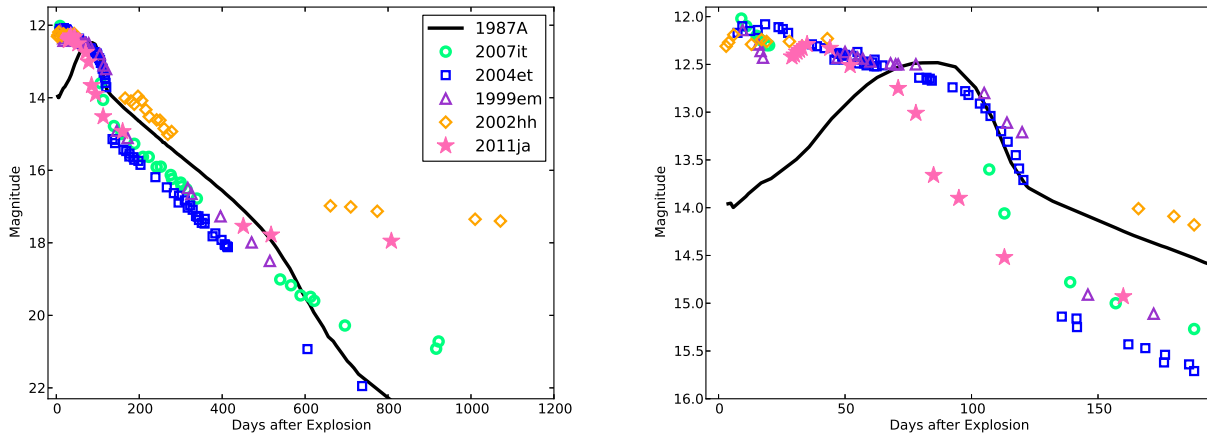


Figure 3. Optical I-band lightcurves for a sample of Type II SNe. The right figure shows a zoomed-in region of the first 200 days. Data are from: SN 1987A (Hamuy et al. 1988; Suntzeff et al. 1988; Hamuy & Suntzeff 1990), SN 2007it (Andrews et al. 2011a), SN 2004et (Sahu et al. 2006), SN 1999em (Elmhadi et al. 2003), and SN 2002hh (Pozzo et al. 2006)

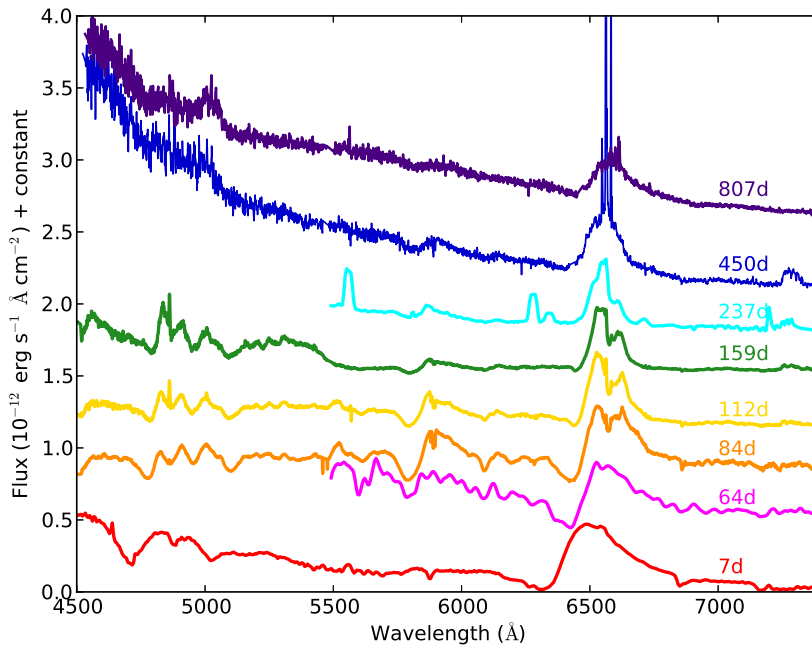


Figure 4. Optical spectra of SN 2011ja. Day 7, 64, and 237 are from NTT/EFOSC2, and the rest are from Gemini/GMOS. All spectra have been flux calibrated but shifted by a constant for presentation. An extinction correction of $E(B-V) = 1.8$ has been applied to all spectra.

what we see in our $H\alpha$ emission lines. Those authors attributed this emission to unshocked ejecta composed of oxygen core material coupled with a low hydrogen envelope mass.

By days 159 and 237, when the SN is well into the nebular phase, the strong P-Cygni profile in $H\alpha$ has all but disappeared. In addition to having multiple peaks, the $H\alpha$ (and to some extent $H\beta$) lines begin to show signs of flattening as the nebular phase persists. Boxy, flat-topped spectra have also been seen in SNe 1993J (Matheson et al. 2000), 1998S (Leonard et al. 2000), 2004et (Kotak et al. 2009), and 2007od (Andrews et al. 2010), and are attributable to CSM interaction. Also noticeable in the $H\alpha$ emis-

sion is the degradation of the red peak from the day 64 and 84 observations (Figure 5). Over the course of ~ 180 days, the ratio of the blue and red peak emission has evolved from 1:1 to 2:1. Further comparison between $H\alpha$ emission of SN 2011ja at \sim day 84, SN 2004dj at day 128, and SN 2007od at day 232 (Figure 6) shows similar structures, particularly in the peaks at ± 1500 km s^{-1} . This double-peaked structure was attributed to the interaction of the ejecta with a torus or disc of material surrounding the supernova, with the stronger attenuation on the red side due to dust forming in the line of sight. The extra peak at $+3200$ km s^{-1} is more of a mystery. It is possible that the multiple peaks seen in the

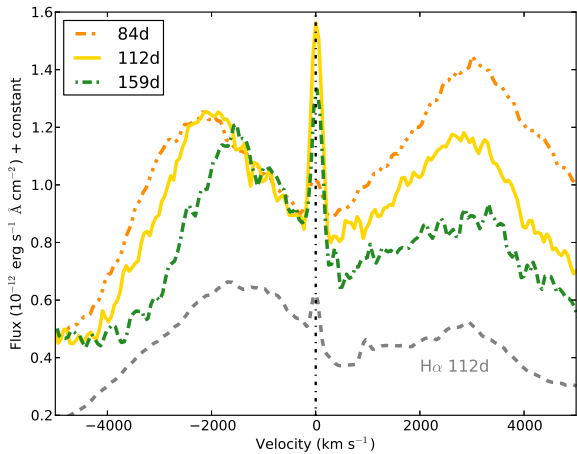
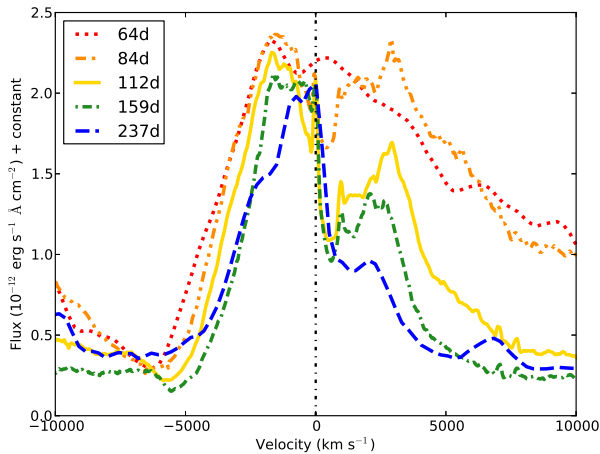


Figure 5. $H\alpha$ (top) and $H\beta$ (bottom) evolution for a subset of epochs from Figure 4. The enhanced red emission in $H\beta$ on day 84 could be due a blend with $\text{Fe } \lambda 4924 \text{ \AA}$.

hydrogen lines could come from asymmetries in ^{56}Ni in the ejecta. This non-uniformity could cause uneven ionization and excitation in the ejecta, as was suggested for the He I lines in the Type IIb SN 2008ax (Taubenberger et al. 2011).

The $H\alpha$ line width of 5000 km s^{-1} persists from day 64 until our last observation on day 807. Late-time spectra show the emergence of strong lines of [N II] $\lambda\lambda 6548, 6583$ and [S II] $\lambda\lambda 6716, 6731 \text{ \AA}$ (see Figure 4). More striking is the blue continuum that emerged in the last two epochs. This occurred at the same time as the leveling off of the optical lightcurve discussed in section 3.2. The two are likely caused by the same phenomenon, and are discussed in detail in Section 5.3.

3.4 IR Observations

In Figure 2 we also show the first ~ 300 days of JHK evolution, including a maximum around day 40. Between day 8 and 40 there is an increase in the absolute magnitude of all NIR bands, although the largest increase of 1.5 mag occurred in the H-band. In the weeks following the maximum there is a steep decline, very similar to the optical lightcurve evolution, until day 121. Between day 121 and 243 the K-band brightens by ~ 0.4 magnitudes and an almost con-

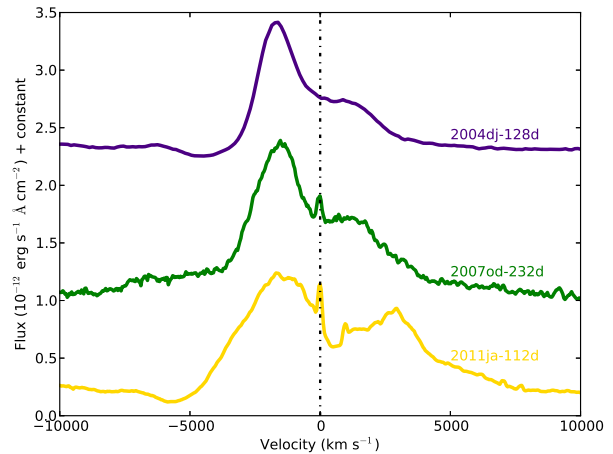


Figure 6. $H\alpha$ profiles of other SNe with known CSM interaction. Data are from Andrews et al. (2010) (2007od) and Vinkó et al. (2006) (2004dj). All three SNe were classified as normal Type II, yet all three show the same double-peaked emission profile, with a dominant blue-peak within 4-8 months post-explosion.

stant plateau in the H-band. This corresponds to the same time period when we believe there was an increase in optical fading by 0.5 magnitudes, and that the $H\alpha$ emission showed the most red-side attenuation. A similar increase in the H- and K-bands was observed around day 50 in SN 2005ip (Fox et al. 2009) and SN 2006jc (Smith et al. 2008). In both cases, the increase in the NIR can be attributed to dust grain formation. Although there is no NIR photometry available to us after day 272, the brightness is once again declining into a radioactive tail, indicating that the new grains have either been destroyed in the reverse shock or have cooled sufficiently to only be detectable at longer wavelengths.

3.5 ^{56}Ni Mass Estimates

We estimate a ^{56}Ni mass for SN 2011ja of $M_{\text{Ni}} = 0.22 \pm 0.03 M_{\odot}$ employing the methods of Hamuy (2003), using the V magnitude at day 84. The bolometric luminosity of the radioactive tail (in erg s^{-1}) is calculated as

$$\log_{10} L_t = \frac{-[V_t - A(V) + BC] + 5 \log_{10} D - 8.14}{2.5}, \quad (1)$$

with $A_V = 5.6$ mag, and a bolometric correction of $BC = 0.26$. The nickel mass is then calculated at various times during this phase, as

$$M_{\text{Ni}} = (7.866 \times 10^{-44}) L_t \exp\left[\frac{t_t - t_0}{111.26} - 6.1\right] M_{\odot}. \quad (2)$$

Here 6.1 days is the half-life of ^{56}Ni and 111.26 days is the e-folding time of ^{56}Co and $t_t - t_0$ is the age of the SN. This calculated Ni mass is much larger than other Type IIP SNe. There is, of course, some uncertainty in the extinction correction, not to mention the luminosity at each epoch could be underestimated due to additional dust formation or overestimated due to circumstellar interaction. If this is an accurate measurement of the ^{56}Ni mass, it would put SN 2011ja in a regime of high mass normally reserved for stripped envelope CCSNe, particularly IIb and Ib (Lyman et al. 2014). For comparison, other “normal” Type IIP SNe such as SNe 1999em, 2003gd, and 2004dj each have ^{56}Ni masses $\sim 0.02 M_{\odot}$, or a full or-

der of magnitude lower than estimated here (Elmhamdi et al. 2003; Hendry et al. 2005; Vinkó et al. 2006).

4 RADIATIVE TRANSFER MODELING

To determine the amount and type of dust being formed in SN 2011ja, we have used the MOCCASIN 3D Monte Carlo radiative transfer code (Ercolano et al. 2005, and references therein). As was done for SN2007it (Andrews et al. 2011a) and SN 2010jl (Andrews et al. 2011b) we assume three different dust geometries. The “smooth” distribution describes dust distributed uniformly within a spherical shell surrounding the SN. The “torus” model distributes dust uniformly within a torus at some inclination around the SN. Finally, the “clumpy” model places dust in clumps and scatters it throughout a spherical shell surrounding the SN. For grain sizes we are using a standard MRN grain size distribution of $a^{-3.5}$ between 0.005 and 0.05 μm (Mathis et al. 1977). For each epoch, we use the Spitzer IRAC data to set the date, and extrapolate the optical and NIR photometry from the surrounding observations. We also correct all photometric points for the assumed $E(B-V)=1.8$.

Continuing on in the manner presented in Andrews et al. (2010, 2011a,b), the dust and luminosity for the source was located between an inner radius R_{in} and an outer radius R_{out} of a spherically expanding shell, with the diffuse emission luminosity being proportional to the density at each location. The smooth model assumes the density of dust in the shell was inversely proportional to the square of the radius. For the clumpy model the photons originate in the inhomogeneous interclump medium, where the clumps are considered to be optically thick and spherical. For the torus models, densities are specified for the inner and outer walls, with the dust distribution falling off linearly between the two radii (Ercolano et al. 2007). For each model we used grains of amorphous carbon (AC) using the optical constants of Hanner (1988), due to the lack of mid-IR detection at 10.8 μm , which would have indicated a strong silicate component. Inputs for the models were luminosity, ejecta temperature, inner and outer radii, and dust masses. For each epoch and parameter, initial estimates were accomplished using blackbody fits to the optical and IR data (solid curves Figure 7). This yielded dust temperatures (T_d) of roughly 550 K for the first epoch (day 105), and 725K for the remaining epochs. These temperatures are consistent with typical warm dust temperatures. Inputs and outputs for each epoch and geometry are listed in Tables 5 and 6.

For the shell models, the first epoch (day 105) is best fit by an R_{in} of 5.3×10^{16} cm, which roughly corresponds to the evaporation radius of the initial flash of the SN. Epochs 2 and 3 (day 486 and 637 respectively) used an R_{in} of 4.5×10^{15} cm, and for our final epoch (day 857) $R_{in} = 3.8 \times 10^{15}$ cm. For the torus models, the best fits were achieved with slightly different values for R_{in} . On day 105 we assumed $R_{in} = 5.0 \times 10^{15}$ cm, and for the remaining epochs $R_{in} = 9.0 \times 10^{15}$ cm. We also kept the temperature of the ejecta (T_{ej}) at 7000K for all epochs, since this is a reasonable ejecta temperature (Sugerman et al. 2006) and does an adequate job fitting the first epoch of optical points. The combination of strong H α and [O I] emission lines in the R band relative to the continuum, and at later times the additional blue flux has made it unlikely that the visible photometry is consistent with any reasonable blackbody temperature. Keeping those two values constant, we then varied the luminosity, dust masses, and for the torus models the number density along the inner edge to get the most accurate fits. For all epochs we found that the clumpy distribution predicted on average about a

factor of two higher dust masses than the smooth and torus models. We have also found that varying the grain sizes and exponent on the grain distribution alters the dust mass outputs. In general increasing the minimum grain size does not alter the dust mass, increasing the exponent integer on the grain size distribution will decrease the dust mass, and increasing the maximum grain size from 0.05 μm to 1 μm will increase dust mass by roughly a factor of two. These values are within the range of masses created by varying the dust geometries (Table 6), which is our largest source of uncertainty. A recent in-depth study presented in Bevan & Barlow (2015) finds that a MRN distribution could not reproduce the line profiles of SN 1987A at early epochs, but as the grain size distribution is not our largest source of uncertainty we retain our standard MRN distribution for consistency.

We estimate a dust mass for our first epoch of $1.0 \times 10^{-4} M_{\odot}$ for the smooth model, $1.9 \times 10^{-4} M_{\odot}$ for clumpy, and $1.4 \times 10^{-4} M_{\odot}$ for the torus. The remaining epochs yielded smooth dust masses of $6.7 \times 10^{-5} M_{\odot}$ for day 486, $6.0 \times 10^{-5} M_{\odot}$ for day 637, and $3.8 \times 10^{-5} M_{\odot}$ for day 857. The larger dust mass from the first epoch is likely due to the flash heating of pre-existing CSM dust that is just outside of the shock radius, and is roughly 200K cooler than the newly formed dust in following epochs. On day 105, the maximum distance the shock could have traveled assuming a velocity of 11000 km s^{-1} is 1×10^{16} cm making this scenario entirely plausible. Additionally R_{in} for this first epoch is larger than R_{out} for the remaining epochs, indicating a different location of the modeled dust. This dust will cool and the IR echo will fade over the next year, so that by the time of Epoch 2, the SED should be dominated by newly formed ejecta dust.

Around the time of Epoch 2, the ejecta should have traveled an average distance of 2.5×10^{16} cm (assuming a late-time expansion of 6000 km s^{-1} measured from H α widths.) This places the IR emission, and therefore the newly formed dust, mostly in the CDS interior to the point of CSM interaction. Of course this is just the SN envelope that is traveling at this velocity. The metal-rich core material itself is likely moving much slower, closer to the 1500 km s^{-1} seen in SN 1987A (McCray 1993), and will only be at a distance of 6.3×10^{15} cm. The steady decline of estimated dust masses over all of the epochs is most likely due to the dust in the distant CSM responsible for the IR echo cooling, leaving only the newly formed dust as the main near-IR contributor. It is also possible that as the reverse shock propagates in Epochs 3 and 4 it destroys the dust that was formed in the CDS between Epochs 1 and 2, or that some of the newly formed dust has cooled as well. This is fully consistent with the picture presented in the spectral evolution.

On day 105, the MOCASSIN models predict a $\tau_v = 0.03$. Using methods presented in Fox et al. (2009), we can also independently estimate the optical depth. If we assume $L_{max} = 1.25 \times 10^9 L_{\odot}$ for SN 2011ja based on the lightcurve maximum, then $E \sim 1.25 \times 10^{49}$ erg using the estimates of SN 2005ip and our previous estimation of SN 2007it. We can constrain the IR energy using the black body fits, which results in an L_{bb} of $5.6 \times 10^6 L_{\odot}$ and therefore an IR energy over the first 105 days of 1.97×10^{47} erg. Inserting these numbers into $\tau \sim \frac{E_{IR}}{E_{IR}+E}$, we calculate a $\tau = 0.015$, consistent with our MOCASSIN fits.

An increase in τ_v between epochs 1 and 2, as mentioned above, occurs coincidentally with the emission line and optical lightcurve extinction, and therefore the formation of new dust. While the total dust mass is actually smaller in the second epoch, the volume into which it is contained is much smaller as well, since R_{out} has decreased by over a magnitude between the two, requiring similar amounts of dust in a much smaller volume. This region

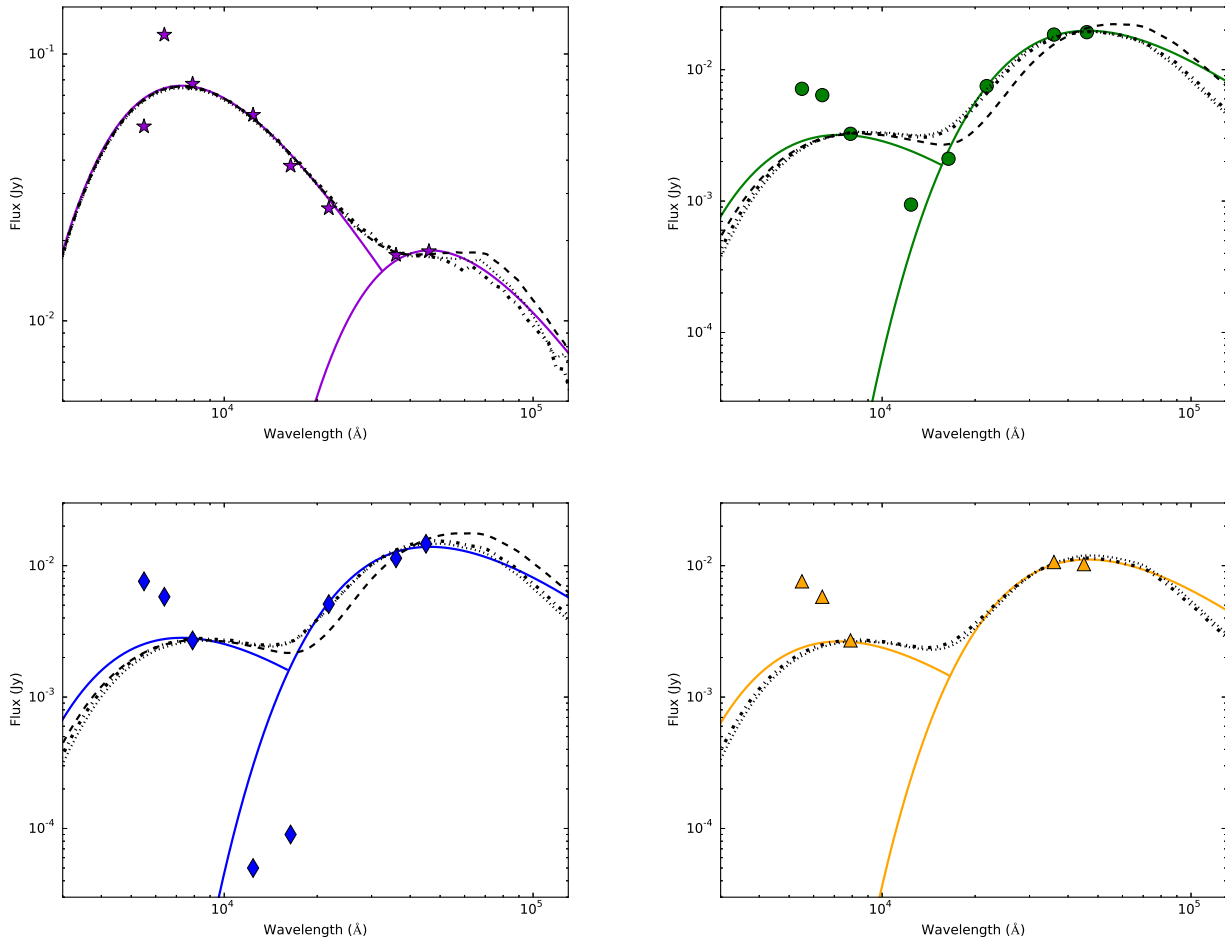


Figure 7. SEDs of days 105 (upper left), 486 (upper right), 637 (lower left), and 857 (lower right). All photometric points have been corrected for $E(B-V)=1.8$, and optical and NIR fluxes have been extrapolated from other observations to match the Spitzer observation dates. Blackbody fits are shown as solid lines. Moccasin fits are shown in dashed (smooth), dotted (torus, 45°), and dash-dotted (clumpy). Note the y-scale is different for Epoch 1 than for the other Epochs.

Table 5. Monte Carlo Radiative Transfer Shell Models

| Epoch | T_{ej} (K) | R_{in} (cm) | R_{out} (cm) | $L_{tot.}$ (L_\odot) | τ_v | Smooth M_d (M_\odot) | Clumpy M_d (M_\odot) |
|-------|--------------|---------------|----------------|--------------------------|----------|-------------------------------|-------------------------------|
| 105 d | 7000 | $5.3e16$ | $5.3e17$ | $1.8e8$ | 0.03 | $1.0e-4$ | $1.9e-4$ |
| 486 d | 7000 | $4.5e15$ | $4.5e16$ | $1.3e7$ | 2.60 | $6.8e-5$ | $1.4e-4$ |
| 637 d | 7000 | $4.5e15$ | $4.5e16$ | $1.0e7$ | 2.34 | $6.1e-5$ | $1.2e-4$ |
| 857 d | 7000 | $3.8e15$ | $4.2e16$ | $9.1e6$ | 1.76 | $3.9e-5$ | $8.6e-5$ |

Table 6. Monte Carlo Radiative Transfer Torus Models

| Epoch | T_{ej} (K) | R_{in} (cm) | R_{out} (cm) | $L_{tot.}$ (L_\odot) | Face-On (0°) | | 45° | | Edge-On (90°) | |
|-------|--------------|---------------|----------------|--------------------------|-----------------------|---------------------|------------|---------------------|------------------------|---------------------|
| | | | | | τ_v | M_d (M_\odot) | τ_v | M_d (M_\odot) | τ_v | M_d (M_\odot) |
| 105 d | 7000 | $5.0e16$ | $5.0e17$ | $1.8e8$ | 0.0 | $1.3e-4$ | 0.03 | $1.5e-4$ | 0.05 | $1.8e-4$ |
| 486 d | 7000 | $9.0e15$ | $4.0e16$ | $1.3e7$ | 0.0 | $4.8e-5$ | 0.0 | $6.1e-5$ | 3.31 | $7.7e-5$ |
| 637 d | 7000 | $9.0e15$ | $4.0e16$ | $9.8e6$ | 0.0 | $4.3e-5$ | 0.0 | $5.4e-5$ | 2.94 | $6.8e-5$ |
| 857 d | 7000 | $9.0e15$ | $4.0e16$ | $8.9e6$ | 0.0 | $3.5e-5$ | 0.0 | $4.3e-5$ | 2.37 | $5.5e-5$ |

is also almost entirely interior to the original R_{evap} , again pointing to newly formed grains. In Section 3.2 we estimate an increase in A_v of 0.5 between day 84 and 112, model results would therefore indicate that the most likely dust geometry would be in a torus inclined at roughly 45° . As can be seen in Table 6, between face-on and 45° , $\tau = 0$, but increases from 0.5 to 3.31 for inclinations between 47 - 90° . Overall, the total mass of new, warm dust formed in SN 2011ja appears to be $\sim 6.0 \times 10^{-5} M_\odot$ by day 857, which although consistent with dust masses of other CCSNe, is still considerably smaller than the amount needed to account for the dust seen at high- z (Morgan & Edmunds 2003). Although in the Introduction, we have described the much larger dust masses seen at longer wavelengths for SN1987A and other SNe observed at much later epochs.

5 DISCUSSION

5.1 Circumstellar Interaction and Environment

The expansion of the supernova shock into the surrounding environment can create X-ray emission if the CSM is dense enough. Chakraborti et al. (2013) found that the X-ray flux in SN 2011ja increased by over a factor of 4 between day 29 and day 113 which was attributed to the supernova interacting with a CSM created from a non-steady wind. As discussed in detail above, the optical spectral evolution implies that CSM interaction is occurring by day 84 and persists onward, agreeing with the X-ray observations. In particular, Chakraborti et al. (2013) hypothesize the progenitor underwent a blue supergiant (BSG) phase shortly before explosion, producing a low density cavity immediately surrounding the SN. Other CCSNe showing an increase in X-ray emission over the first 120 days include the type IIP SN 1999em (Pooley et al. 2002) and the type Ib SN 2006jc (Immler et al. 2008), and both instances were attributed to shock interaction with the CSM.

If we use the optical spectra to constrain the date of the onset of shock interaction, we can safely assume that while it was already beginning on day 64, it was fully occurring by day 84. Assuming the initial expansion velocity of $11\,000 \text{ km s}^{-1}$ was sustained, the CSM is located $8 \times 10^{15} \text{ cm}$ away from the SN. On day 113, when the X-ray observation was taken, the shock had reached a maximum distance of 10^{16} cm .

It is important here to remark on the evaporation radius (R_{evap}), the cavity cleared by the explosion of the supernova. Following the evaporation radii computed by Fransson et al. (2014) for SN 2010jl, we have estimated the ranges of R_{evap} from grain size and type. Using an absolute magnitude of $I = -18.3$, and standard bolometric correction of 0.26, we estimate $L_{max} = 4.8 \times 10^{42} \text{ erg s}^{-1}$, or $1/6^{th}$ the maximum luminosity of SN 2010jl. This means that for graphite grains (which are used in our MOCASSIN models), and a $T_{eff} = 10^4$, $R_{evap} = 2.4 \times 10^{16}$ and $9.0 \times 10^{16} \text{ cm}$ for $1.0 \mu\text{m}$ and $0.001 \mu\text{m}$, respectively. Therefore we can reasonably assume an $R_{evap} = 5 \times 10^{16} \text{ cm}$. If of course the BC or E(B-V) estimations are under- or over- estimated this radius can change. A lower L_{max} of $1 \times 10^{42} \text{ erg s}^{-1}$ could bring R_{evap} as close as 10^{16} cm , which was the R_{evap} estimated for SN 2005ip (Fox et al. 2010) and SN 2007it (Andrews et al. 2011a). Additionally, a clumpier CSM could also allow grains to survive closer to the SN. Therefore, R_{evap} is consistent with the CSM interaction beginning by day 84.

As mentioned above, an intermediate-width [O III] emission line of $\sim 3000 \text{ km s}^{-1}$ may be visible in our day 84 spectra and persist up to the last spectral observation. According to Fransson et al.

(2002), if the explosion is asymmetric it is possible to get [O III] $\lambda 5007$ emission at early times. The scenario described for a similar feature seen in the Type II SN 1995N is that the intermediate component is actually the oxygen core of the supernova. The presence of this line also may help explain the interesting shape of the hydrogen lines. To get high enough ionization energies an asymmetric explosion, with most of the energy occurring in the plane, is needed. This would create a slower expansion velocity along the plane and much faster in the polar direction. This scenario could explain the intermediate-width $H\alpha$ and $H\beta$ lines as well, which have an underlying broad component coming from the polar region.

5.2 New Dust Formation and Location

Over the past few years it has become apparent that there are two modes of dust formation in CCSNe. If there is strong CSM interaction occurring it is possible for dust grains to condense in the cool dense shell (CDS) between the forward and reverse shocks. This has been seen in other SNe such as SN 1998S (Pozzo et al. 2004), SN 2004dj (Meikle et al. 2011), SN 2005ip (Fox et al. 2009; Smith et al. 2009), SN 2006jc (Smith et al. 2008), SN 2007od (Andrews et al. 2010), and SN 2010jl (Smith et al. 2012; Gall et al. 2014). Taken solely on the formation of grains within the first 150 days of explosion in SN 2011ja would point to dust formation in the CDS. The appearance of asymmetrical hydrogen lines in the optical spectra is a smoking-gun. We cannot rule out the possibility of small amounts of dust forming in the expanding ejecta at later times, but observational evidence points to new dust forming between day 84 - 112 in a region between 4.5×10^{15} and $4.5 \times 10^{16} \text{ cm}$ away.

5.3 Late-time luminosity

After day 400 there is little change to the luminosity of SN 2011ja in VRI. There are three possibilities to this late-time brightness: a) a scattered light echo off the surrounding CSM, b) radiative shocks, or c) fading of the SN into the ambient brightness of the parent cluster. These three possibilities are not mutually exclusive. Scattered light echoes occur when light from the supernova scatters off circumstellar or interstellar dust and redirects it back into the line of sight of the observer at some later time. The scattering is more efficient at shorter wavelengths, causing the light echo spectrum to look bluer than the peak SN light. At the same time, a leveling out of the optical lightcurve is created as the original light pulse travels outward through the intervening material creating a constant luminosity. The late time spectra, SED, and lightcurve all show indications that this could be a possibility, as the spectrum becomes bluer and the light curve flattens out. The inference of pre-existing dust from the SED modeling as well as the high level of extinction in the direction of SN 2011ja also imply that there is plenty of intervening circumstellar and interstellar dust to create light echoes. Unfortunately, when one creates a light-echo spectrum of the SN using the integrated fluency from the spectra prior to day 100, similar to that done for SN 1980K in Sugerman et al. (2012) while the emission lines appear similar, there is not enough flux in the blue to create a match (Figure 8). So while a light echo may be present, it would be much fainter than the late-time spectrum presented here, so we have ruled this out as the cause of the late-time luminosity. A caveat to this assumption is that the SN explosion date could be earlier than estimated here, which would mean the inclusion of an earlier, bluer light echo spectrum. Deep HST imaging of the region around SN 2011ja could resolve a scattered light echo if one exists.

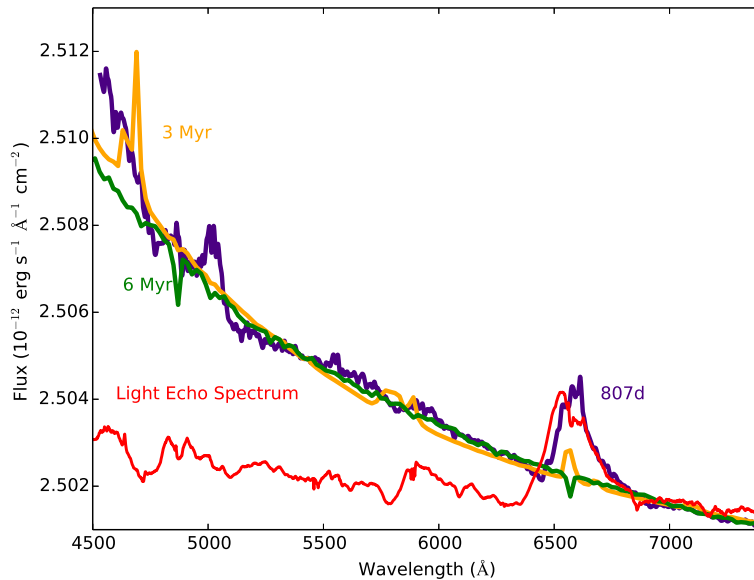


Figure 8. Day 807 spectrum (purple) of SN 2011ja showing enhanced blue emission. Comparison with the light echo spectrum created from an integrated fluency of the first 84 days (red) indicates that a light echo cannot be responsible for the flux blueward of 6000Å. The orange and yellow spectra are synthesized stellar populations created with Starburst99 for 3 and 6 Myr. It is possible that the late-time luminosity has a large component of the parental stellar cluster.

The second scenario requires dense CSM to convert the kinetic energy of the expanding supernova into radiation via shocks. This is a fairly common occurrence in Type II_n SNe at early times, and seems to be more common than originally observed in normal Type II as observations are extending past the first 3 months after explosion. By day 807, the bulk of the SN ejecta will have reached a distance of 4.1×10^{16} cm (or 7.7×10^{16} for the fastest moving ejecta). This places the edge of the ejecta clearly outside of R_{evap} , and at the distance of the CSM responsible for the early IR luminosity, making radiative shocks plausible. Unfortunately a shock driven luminosity, while theoretically being responsible for the constant light curve, would not make the optical spectrum bluer. Additionally, the CSM should slow the ejecta expansion, and there does not seem to be a substantial decrease in the expansion speeds in $H\alpha$ from day 450 to day 807. Therefore we assume that radiative shocks are not responsible for the late time optical plateau, although additional X-ray observations could potentially reveal if CSM interaction is indeed occurring.

Since only $\sim 5\text{--}10\%$ of massive stars are formed in isolation (Oey et al. 2013), it would not be out of the question to detect a CCSN still located in the stellar cluster from which it is formed that would become detectable as the SN faded. For instance, the type IIP SN 2004dj occurred in the massive cluster Sandage-96 and showed very similar late-time photometric and spectroscopic evolution as SN 2011ja (Vinkó et al. 2009). The lightcurves leveled out after day 800 to the magnitude of the cluster in pre-explosion HST images. The spectrum also showed a very blue continuum below 6000 Å, but the nebular features of the SN ($H\alpha$, [O I]) are still present in the red part of the spectrum. Inspection of the day 807 Gemini images indicate that the size of the emitting object at the SN location is $\leq 1.7''$, or 16 pc at the distance of SN 2011ja. Unfortunately the faintness of the object accompanied by poor seeing makes it difficult to get an accurate FWHM of the object. The average effective radii of stellar clusters are ~ 4 pc, but cluster radii, especially for

younger clusters, can extend out to 15-20 pc (Larsen 2004), making it possible that we are indeed seeing a stellar cluster+SN. As discussed in more detail below and shown in Figure 8, comparison with Starburst99 stellar synthesis models (Leitherer et al. 1999) of solar metallicity give us a decent fit with a 3-6 Myr cluster with the same intrinsic extinction of $E(B-V) = 1.8$. While we cannot definitively rule out the other two options, the late-time luminosity may be largely due to the bright parental cluster of SN 2011ja.

5.4 Progenitor Characteristics

Mass loss estimates for the progenitor of SN 2011ja on day 29 and 113 derived from X-ray fluxes were presented in Chakraborti et al. (2013). Using the narrow $H\alpha$ emission component present in our day 84 spectrum, we estimate the velocity of the surrounding medium to be ~ 180 km s^{-1} , using the FWHM. This is of course the limiting resolution of the spectra, suggesting that this velocity is only an upper limit. The true value could be an order of magnitude lower and more closely resemble RSG wind speeds. This would mean a mass loss of $2 \times 10^{-7} - 10^{-6} M_{\odot}$ on day 29 and $3 \times 10^{-6} - 10^{-5} M_{\odot}$ on day 113, values consistent with BSG and RSG mass-loss rates respectively. For comparison HD 168625 is a BSG with measured stellar winds of ~ 183 km s^{-1} and $\dot{M} = 1.2 \times 10^{-6} M_{\odot}$ (Nota et al. 1996) and SBW1, a near twin of the progenitor of SN 1987A, has an estimated mass loss of $3 \times 10^{-7} M_{\odot}$ (Smith et al. 2013). Therefore as hypothesized by Chakraborti et al. (2013), it is likely that the increase in X-ray luminosity could be explained by the supernova initially expanding into a low-density region then encountering a high-density RSG-like environment caused by a RSG going through a blue-loop before returning to a RSG phase. If the RSG mass-loss had a density enhancement in the equatorial region, this could also allow for easy expansion in the polar directions, while further increasing the density of the circumstellar ring via shocks.

There are other possible explanations for the presence of significant, asymmetric CSM close to the SN. For example the two BSGs listed above, along with Sher25 are all LBV candidates with triple ring structures and more importantly, all have a central ring surrounding the star. It is possible that the environment created around these stars was caused by a violent LBV or BSG eruption, not density enhancements from RSG winds (Hendry et al. 2008; Smith 2007; Smith et al. 2013). It is also possible that the progenitor was a more massive RSG that underwent episodic mass loss, creating shells as the faster, less-dense material runs into the slower, denser material (Smith et al. 2009; Mauerhan et al. 2013). The major factor in all of these scenarios is the inferred initial mass of the progenitor. For an RSG we would expect a progenitor mass $< 25 M_{\odot}$ (Levesque et al. 2005), whereas for LBVs we could have masses as great as 40-60 M_{\odot} . While originally classified as a normal Type IIP SNe, it is possible that like PTF11iqb (Smith et al. 2015), SN 2011ja was actually a Type IIn for a very brief stage. This could allow for the possibility of a much larger progenitor, as it is generally thought that IIn SNe come from LBV or massive RSG stars. The explosion date of 2011 December 12 is only an estimate, though likely a well constrained one, and it is possible that the first observed spectrum could be multiple days older than the projected 7 days. PTF11iqb lost the narrow IIn features ~ 14 days after explosion, and any delay in its discovery would have classified it as a normal Type II.

Figure 8 shows the day 807 spectrum fit by both a 3 Myr and 6 Myr cluster model with solar metallicity produced by Starburst99. Without higher S/N and more accurate flux calibration it is impossible to put strict limits on the cluster age and therefore progenitor mass. Extensive stellar synthesis modeling and age-dating is beyond the scope of this paper, but the spectrum does seem to agree with a 3-6 Myr cluster and a progenitor mass $\geq 25 M_{\odot}$. Using high-resolution Keck LRIS spectroscopy, Vinkó et al. (2009) estimate that SN 2004dj had a 10-20 M_{\odot} progenitor and resided in a 10-20 Myr old cluster. More recently Kuncarayakti et al. (2013) determined a cluster age of 15.6 Myr, corresponding to a mass of 14.7 M_{\odot} . One notable difference is the lack of $H\alpha$ emission around Sandage-96, whereas pre-explosion $H\alpha$ imaging of NGC 4945 from the Danish 1.54m telescope indicates strong emission at the location of SN 2011ja (Rossa & Dettmar 2003). $H\alpha$ emission can be a strong indicator of cluster age, and is not commonly found in clusters with an age > 8 Myr (Andrews et al. 2013). Strong $H\alpha$ emission was also seen around SN 2010jl, and archival HST imaging may point to a natal cluster < 7 Myr and progenitor mass $> 30 M_{\odot}$ (Smith et al. 2011). It is also interesting to note that the BSG Sher25 above may also reside in a ~ 4 Myr old cluster (Melena et al. 2008).

Chakraborti et al. (2013) conclude the progenitor to SN 2011ja must be a RSG with a mass $\geq 12 M_{\odot}$ assuming that the X-ray variations are only due to a density enhancement by a BSG wind and that SN 2011ja was a normal Type IIP SN. The combination of parent cluster age and $H\alpha$ retention and ^{56}Ni mass presented here, combined with previous X-ray observations all point to a larger progenitor mass for SN 2011ja than usually attributed to Type IIP SNe. This could be of notable importance since to date, observational evidence only suggests RSG progenitor masses of Type IIP SNe of up to $\sim 16 M_{\odot}$, the so-called “red supergiant problem” (Smartt et al. 2009; Smartt 2015). Hypotheses for this mismatch range from underestimation of dust extinction (Walmswell & Eldridge 2012), stellar evolutionary limits (Groh et al. 2013), or direct collapse to black holes with little to no optical emission (Lovegrove & Woosley 2013, Kochanek 2014). Smith et al. (2011)

suggest that the high mass RSGs may actually continue to evolve into blue or yellow supergiants or Wolf-Rayet stars prior to core collapse, forming other CCSNe (IIL, IIn, Ibc). This can be done either in a single or binary evolutionary track, and not only alleviates the need to invoke direct collapse to a black hole, but is also compatible with the fractional occurrence of non-IIP core-collapse events. If in fact the progenitor of the Type IIP SN 2011ja is in the 20-30 M_{\odot} range it may be one of the first definitive examples of high-mass RSGs giving rise to a CCSNe. Alternatively, the progenitor may be an LBV or a BSG and SN 2011ja may be an example of a Type II SNe discovered after a brief IIn phase.

6 SUMMARY

We have presented a multi-wavelength analysis of SN 2011ja, another normal Type IIP SN, with not so normal evolution. The short optical lightcurve plateau may place SN 2011ja into the realm of objects somewhere between IIP and IIL that have been in the spotlight in recent years. Signatures of dust formation are also seen after day 105, when the NIR flux increases, the $H\alpha$ emission lines become attenuated on the red side, and the optical flux decreases. At the same time there is also a noticeable increase in the X-ray flux (Chakraborti et al. 2013), which is a strong indication of CSM interaction. This is further exemplified by the flat-topped hydrogen profiles in the optical spectra, particularly the $H\alpha$ line. The dust formation, the flat-topped line profiles, and the increased X-ray emission all seem to occur at roughly the same time, which paints a picture of the ejecta of SN 2011ja running into dense CSM about ~ 4 months post-explosion. As the ejecta runs into the CSM an area is then created between the forward and reverse shock region where $\sim 6.0 \times 10^{-5} M_{\odot}$ of dust was quickly formed. It seems SN 2011ja is likely another case of dust formation occurring early on in a CDS.

The asymmetry of the line profiles point to a pre-existing CSM with a density enhancement inclined 30-45 degrees from edge-on. Combined with the possible detection of a young (3-6 Myr) cluster at the location of the SN and the large inferred ^{56}Ni mass of 0.22 M_{\odot} , it is possible that SN 2011ja had 25-30 M_{\odot} LBV or RSG progenitor that suffered a massive outburst prior to eruption. Although LBVs are generally thought to be the progenitors of Type IIn SNe, recently Smith et al. (2015) found that PTF11iqb could have been classified as a normal Type IIP SN had it been discovered just days after the initial classification, as the narrow component quickly disappeared. This could have been the case with SN 2011ja as well. If the surrounding CSM was caused by an outburst, it would have likely gone undetected due to the extreme extinction ($A_v \approx 5.6$) in the SN environment. Deep observations with large ground- or space-based telescopes as SN 2011ja continues to fade will prove essential in putting tighter constraints on the age of the cluster and therefore the mass of SN progenitor.

SN 2011ja seems to share similar properties with the type IIn SNe 1998S and 2005ip, the type Ib/c SN 2006jc, and the type II SNe 2004dj and 2007od. In all cases interaction with dense CSM creates similar observational signatures, and dust formation at early times in the CDS regardless of initial SN classification. Particular similarities between SNe 2011ja, 2004dj and 2007od indicate there is a sub-class of Type IIP SNe that have mass-loss histories capable of producing pronounced observational signatures normally reserved for other CCSNe. This only highlights the need for more late time observations of even the most seemingly mundane objects, as

there seems to be much we do not know about pre-supernova mass loss.

ACKNOWLEDGMENTS This work is based in part on observations from Spitzer Space Telescope and was supported by RSA 1415602 and RSA 1346842, issued by JPL/Caltech. Based on observations obtained at the Gemini Observatory, which is operated by the Association of Universities for Research in Astronomy, Inc., under a cooperative agreement with the NSF on behalf of the Gemini partnership: the National Science Foundation (United States), the National Research Council (Canada), CONICYT (Chile), the Australian Research Council (Australia), Ministério da Ciência, Tecnologia e Inovação (Brazil) and Ministerio de Ciencia, Tecnología e Innovación Productiva (Argentina). We would like to thank the anonymous referee for their insightful comments during the revision of this paper.

REFERENCES

- Anderson, J. P., James, P. A., Habbergham, S. M., Galbany, L., & Kuncarayakti, H. 2015, *PASA*, 32, e019
- Andrews, J. E., et al., 2010, *ApJ*, 715, 541
- Andrews, J. E., et al. 2011a, *ApJ*, 731, 47
- Andrews, J. E., et al. 2011b, *AJ*, 142, 45
- Andrews, J. E., et al., 2013, *ApJ*, 767, 51
- Arcavi I., et al., 2012, *ApJ*, 756, L30
- Bevan, A., & Barlow, M. J. 2015, arXiv:1509.00858
- Barlow M. J., et al., 2010, *A&A*, 518, L138
- Cardelli J. A., Clayton G. C., Mathis J. S., 1989, *ApJ*, 345, 245
- Chakraborti S., et al., 2013, *ApJ*, 774, 30
- Chevalier R. A., Fransson C., Nyman T. K., 2006, *ApJ*, 641, 1029
- Chugai N. N., Chevalier R. A., Utrobin V. P., 2007, *ApJ*, 662, 1136
- Draine, B. T., Dale, D. A., Bendo, G., et al. 2007, *ApJ*, 663, 866
- Dwek E., Staguhn J., Arendt R. G., Kovacks A., Su T., Benford D. J., 2014, *ApJ*, 788, L30
- Elmhamdi A., et al., 2003, *MNRAS*, 338, 939
- Ercolano B., Barlow M. J., Storey P. J., 2005, *MNRAS*, 362, 1038
- Ercolano B., Barlow M. J., Sugerman B. E. K., 2007, *MNRAS*, 375, 753
- Fox O., et al., 2009, *ApJ*, 691, 650
- Fox, O. D., et al. 2010, *ApJ*, 725, 1768
- Fransson C. et al., 2002, *ApJ*, 572, 350
- Fransson C., et al., 2005, *ApJ*, 622, 991
- Fransson C., et al., 2014, *ApJ*, 797, 118
- Galametz, M., et al. 2011, *A&A*, 532, A56
- Gall C., Andersen A. C., Hjorth J., 2011, *A&A*, 528, A14
- Gall C., et al., 2014, *Nature*, 511, 326
- Gomez H. L., et al., 2012, *ApJ*, 760, 96
- Hamuy M., 2003, *ApJ*, 582, 905
- Hamuy M., Suntzeff N. B., 1990, *AJ*, 99, 1146
- Hamuy M., Suntzeff N. B., Gonzalez R., Martin G., 1988, *AJ*, 95, 63
- Hanner M., 1988, Technical report, Grain optical properties
- Hendry, M. A., et al. 2005, *MNRAS*, 359, 906
- Hendry M. A., Smartt S. J., Skillman E. D., Evans C. J., Trundle C., Lennon D. J., Crowther P. A., Hunter I., 2008, *MNRAS*, 388, 1127
- Immler, et al. 2008, *ApJL*, 674, L85
- Kiewe M., et al., 2012, *ApJ*, 744, 10
- Kotak R., et al. 2009, *ApJ*, 704, 306
- Kuncarayakti H., Doi M., Aldering G., Arimoto N., Maeda K., Morokuma T., Pereira R., Usuda T., Hashiba Y., 2013, *AJ*, 146, 31
- Larsen S. S., 2004, *A&A*, 416, 537
- Lau R. M., Herter T. L., Morris M. R., Li Z., Adams J. D., 2015, arXiv:1503.07173L
- Leitherer C., Schaerer D., Goldader J. D., Delgado R. M. G., Robert C., Kune D. F., de Mello D. F., Devost D., Heckman T. M., 1999, *ApJs*, 123, 3
- Leonard D. C., Filippenko A. V., Barth A. J., Matheson T., 2000, *ApJ*, 536, 239
- Levesque E. M., Massey P., Olsen K. A. G., Plez B., Josselin E., Maeder A., Meynet G., 2005, *ApJ*, 628, 973
- Lucy L. B., Danziger I. J., Gouiffes C., Bouchet P., 1989, in Tenorio-Tagle G., Moles M., Melnick J., eds, IAU Colloq. 120: Structure and Dynamics of the Interstellar Medium Vol. 350 of Lecture Notes in Physics, Berlin Springer Verlag, Dust Condensation in the Ejecta of SN 1987 A. p. 164
- Lyman, J., Bersier, D., James, P., et al. 2014, arXiv:1406.3667
- Maeda, K., et al. 2015, ArXiv e-prints
- Marconi A., Oliva E., van der Werf P. P., Maiolino R., Schreier E. J., Macchetto F., Moorwood A. F. M., 2000, *A&A*, 357, 24
- Matheson T., et al. 2000, *AJ*, 120, 1487
- Mathis J. S., Rimpl W., Nordsieck K. H., 1977, *ApJ*, 217, 425
- Matsuura, M., et al. 2011, *Science*, 333, 1258
- Matsuura, M., 2015, *ApJ*, 800, 50
- Mattila S., et al. 2008, *MNRAS*, 389, 141
- Mauerhan J., et al. 2014, *MNRAS*, 442, 1166
- Mauerhan J. C., et al., 2013, *MNRAS*, 430, 1801
- Mauron N., Josselin E., 2011, *A&A*, 526, A156
- McCray R., 1993, *ARA&A*, 31, 175
- Meikle W. P. S., et al., 2007, *ApJ*, 665, 608
- Meikle W. P. S., et al., 2011, *ApJ*, 732, 109
- Melena N. W., Massey P., Morrell N. I., Zangari A. M., 2008, *AJ*, 135, 878
- Michałowski, M. J. 2015, *A&A*, 577, A80
- Monard, L. A. G., et al. 2011, Central Bureau Electronic Telegrams, 2946, 1
- Morgan H. L., Edmunds M. G., 2003, *MNRAS*, 343, 427
- Mouchine M., Ferguson H. C., Rich R. M., Brown T. M., Smith T. E., 2005, *ApJ*, 633, 810
- Nota A., Pasquali A., Clampin M., Pollacco D., Scuderi S., Livio M., 1996, *ApJ*, 473, 946
- Oey M. S., Lamb J. B., Kushner C. T., Pellegrini E. W., Graus A. S., 2013, *ApJ*, 768, 66
- Owen P. J., Barlow M. J., 2015, *ApJ*, 801, 141
- Poznanski D., Ganeshalingam M., Silverman J. M., Filippenko A. V., 2011, *MNRAS*, 415, L81
- Poznanski D., Prochaska J. X., Bloom J. S., 2012, *MNRAS*, 426, 1465
- Pozzo M., Meikle W. P. S., Fassia A., Geballe T., Lundqvist P., Chugai N. N., Sollerman J., 2004, *MNRAS*, 352, 457
- Pozzo, M., et al. 2006, *MNRAS*, 368, 1169
- Rossa J., Dettmar R.-J., 2003, *A&A*, 406, 505
- Sahu D. K., Anupama G. C., Srividya S., Muneer S., 2006, *MNRAS*, 372, 1315
- Seaton, M. J. 1979, *MNRAS*, 187, 73P
- Schlafly E. F., Finkbeiner D. P., 2011, *ApJ*, 737, 103
- Slavin J. D., Dwek E., Jones A. P., 2015, *ApJ*, 803, 7
- Smartt S. J., 2015, arXiv:1504.02635S
- Smartt S. J., Eldridge J. J., Crockett R. M., Maund J. R., 2009, *MNRAS*, 395, 1409
- Smith N., 2007, *AJ*, 133, 1034
- Smith N., Arnett W. D., Bally J., Ginsburg A., Filippenko A. V., 2013, *MNRAS*, 429, 1324
- Smith N., Foley R. J., Filippenko A. V., 2008, *ApJ*, 680, 568
- Smith N., Hinkle K. H., Ryde N., 2009, *AJ*, 137, 3558
- Smith N., et al., 2011, *ApJ*, 732, 63
- Smith N., et al., 2015, *MNRAS*, 449, 1876
- Smith N., Mauerhan J. C., Prieto J. L., 2014, *MNRAS*, 438, 1191
- Smith N., et al. 2009, *ApJ*, 695, 1334
- Smith N., Silverman J. M., Filippenko A. V., Cooper M. C., Matheson T., Bian F., Weiner B. J., Comerford J. M., 2012, *AJ*, 143, 17
- Stanghellini, L., Magrini, L., & Casasola, V. 2015, arXiv:1508.02754
- Sugerman B. E. K., et al., 2012, *ApJ*, 749, 170
- Sugerman B. E. K., et al., 2006, *Science*, 313, 196
- Suntzeff N. B., Hamuy M., Martin G., Gomez A., Gonzalez R., 1988, *AJ*, 96, 1864
- Taubenberger, S., et al. 2011, *MNRAS*, 413, 2140
- Temim T., Dwek E., Tchernyshyov K., Boyer M. L., Meixner M., Gall C., Roman-Duval J., 2015, *ApJ*, 799, 158
- Vinkó J., et al. 2009, *ApJ*, 695, 619
- Vinkó, J., et al. 2006, *MNRAS*, 369, 1780

- Welch D. L., Clayton G. C., Campbell A., Barlow M. J., Sugerman B. E. K., Meixner M., Bank S. H. R., 2007, *ApJ*, 669, 525
- Wesson, R., Barlow, M. J., Matsuura, M., & Ercolano, B. 2015, *MNRAS*, 446, 2089
- Wooden D. H., Rank D. M., Bregman J. D., Witteborn F. C., Tielens A. G. G. M., Cohen M., Pinto P. A., Axelrod T. S., 1993, *ApJs*, 88, 477